*Progress In Electromagnetics Research B, Vol. 22, 285–303, 2010*

# INVESTIGATIONS ON AN H-FRACTAL WIDEBAND MICROSTRIP FILTER WITH MULTI-PASSBANDS AND A TUNED NOTCH BAND

**J. M. Patin, N. R. Labadie, and S. K. Sharma**

Department of Electrical and Computer Engineering
San Diego State University
5500 Campanile Drive, San Diego, CA 92182-1309, USA

**Abstract**—This paper investigates an H-fractal wideband microstrip filter with multi-passbands and a tuned notch band for wireless communication frequencies. The four different filter configurations explored are: symmetric with zero offset, symmetric with nonzero offset, asymmetric with zero offset, and asymmetric with nonzero offset. The effect of H-fractal iterations, fractal scaling parameters, and stub offset on the filter's multi-passband response is presented. A comparison is made to a non-fractal straight stub filter of equivalent length showing improved passband bandwidth while maintaining the same overall response. Then an asymmetry is introduced into the fractal geometry to produce a tuned notch band in the second passband. Two fractal scaling factors are shown to aid in the tuning of the filter notch band. Finally, an asymmetric filter is fabricated on FR-4 substrate and experimentally verified, illustrating that the filter has multi-passbands and can find applications in WiFi/WiMAX transponders. The fabricated filter's first two passbands (with respect to $S_{11} = -10\,\text{dB}$) are from 2.09 GHz to 3.18 GHz (fractional bandwidth of 1.09 GHz, 41.36%) and from 4.1 GHz to 5.43 GHz (factional bandwidth of 1.33 GHz, 27.91%), both for WiFi applications along with a notch band ($S_{21} = -3\,\text{dB}$) from 3.3 GHz to 3.94 GHz (factional bandwidth of 0.64 GHz, 17.67%) to suppress co-site WiMAX transmission. The measured data agrees reasonably well with the simulated filter response.

## 1. INTRODUCTION

Fractal geometry has been widely explored in a number of microwave and antenna applications where compactness and multiple resonances

Corresponding author: S. K. Sharma (ssharma@mail.sdsu.edu).

are desirable. Compactness is achieved by maximizing the length of conductive edges within a given space. This is typically realized by a bifurcated or meandered transmission line, or perforated gasket. A fractal is created when these bifurcations, meanderings or perforations are repeated such that the geometry has the self-similar structure at any scale. In practice, only a finite number of fractal iterations are possible and the resulting structure is sometimes called a quasi-fractal. It is these scaled iterations of the structure that produces multiple resonances. The fractal scaling factors can be chosen such that resonances are spaced widely apart or are closely spaced so as to increase the bandwidth of the response.

While fractals have often been applied to antenna design, there has also been considerable interest in applying fractal geometry to microwave filter design. In [1], a coupled line filter is modified by Koch fractal edges to suppress the parasitic second harmonic. The fractal edges compensate for the different even and odd mode phase velocities that produce the unwanted harmonic. The Koch fractal has been used as a defected ground plane resonator to achieve a UWB filter response [2]. In this case, the fractal structure is used mainly for its compactness, and 128% bandwidth is demonstrated. Sierpinski gasket designs have been shown to have very high selectivity and miniaturization when used as coupled resonators [3]. Recently Sierpinski gaskets have also been used in multi-stub multi-bandpass filters resulting in improved passband responses and tuned notch bands [4]. In [5], two microstrip bandpass filters utilizing multi-mode operation and achieving wide pass and stop bands use fractal equilateral triangular patch resonators. The authors are able to achieve up to 48% bandwidth using this structure. There are numerous other examples of fractal which are used to improve a variety of microwave filter characteristics [6–10].

Recently, a single stage H-fractal filter was proposed to achieve widely spaced resonant stop bands [11]. The filter application was derived from the previous work with the H-fractal in photonic band gap [12]. The design in [11] was fabricated on FR-4 substrate of dimensions $30 \times 30\,\mathrm{mm}^2$ and 0.6 mm thickness. Using a $50\,\Omega$ main transmission line and 0.2 mm wide fractal lines, the length of the first fractal level was varied to show the tunability of the filter stop bands. One drawback of the H-fractal filter showed in [11] is the slow roll-off of the passband.

This paper presents detailed investigations of a novel wideband microstrip H-fractal asymmetric bandpass filter providing multi-passbands and a tuned notch band. Section 2 describes the definitions of fractal structural parameters. Section 3 explores fractal iterations

and fractal scaling parameters for a H-fractal filter [11], which is termed in this paper as the symmetric case with zero offset. It is then shown that the filter passband and transition (from pass to stop or stop to pass) bands can be significantly improved by introducing an offset between the two filter stubs. Furthermore, a comparison is made between the offset fractal stubs and non-fractal stubs based filters showing both the improved passband return loss and fractional bandwidth while maintaining the same overall filter response. Section 4 introduces a novel asymmetry into the fractal structure that produces a tuned notch band uniquely within the second passband. The tunability and quality of the notch band is established by sweeping over two scaling parameters, $L_{scale}$ and $R_{scale}$, defined in Section 2. The effect of the stub offset is then explored, which widens the passbands while leaving the notch band unaffected. An equivalent circuit model is developed for the H-fractal filter in Section 5, which is based on the microstrip T-junction circuit model. Finally, in Section 6, circuit modeled, simulated, and measured results for an asymmetric offset fabricated filter are presented, illustrating the filter's possible use in the WiMAX/WiFi transponder applications. The full wave analysis was performed using Ansoft Corporation's Method of Moment (MOM) based Designer and Finite Element Method (FEM) based High Frequency Structure Simulator (HFSS) programs [13].

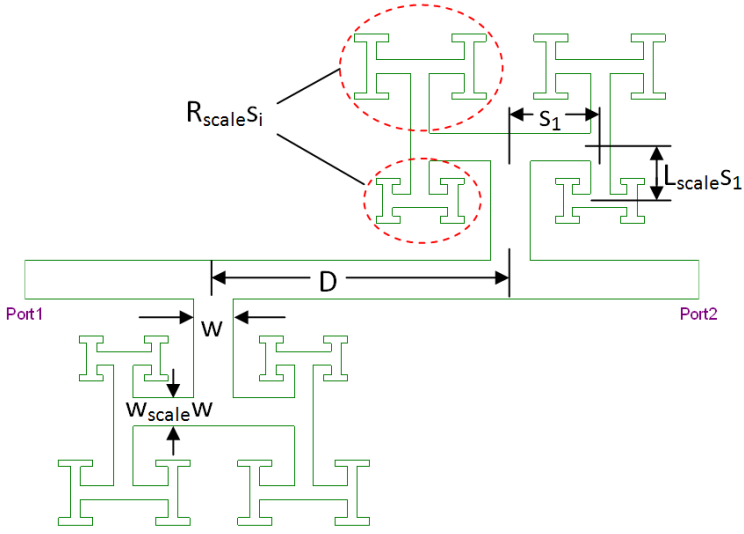


**Figure 1.** The geometry of the microstrip H-Fractal filter showing the filter design parameters.

## 2. FRACTAL ITERATION PARAMETER RESULTS

Referring to Fig. 1, the offset between the fractal stubs is denoted by $D$. The line width is denoted by $w$ which is scaled by $w_{scale}$ at each branching of the fractal at the T-junction. Here, the term "branch" refers to either of the lines that split from the feed line at the T-junction as shown in Fig. 1. The overall length of the fractal stub is set equal to an equivalent quarter wavelength straight stub of length $L_{stub}$. The remaining length of the stub is divided into scaled segments. At each fractal branch, the length of the branched segment is scaled by $L_{scale}$ with respect to the previous feed line and the next branch. Asymmetry is introduced at the second T-junction from the main line where all of the subsequent lengths in the bottom branch are scaled by $R_{scale}$ with respect to those on the top branch. Fractal iteration is defined by the number of T-junctions present in the stub and is illustrated in Fig. 2(a) for the 0th to 5th order iterations. Fig. 2(b) shows the progression of fractal iteration on the $S_{21}$ performance where the total length of the stub is set to a constant value of $\lambda_g/4$ within the substrate. The value of $\lambda_g$ sets the location of the first resonance, which is approximately 1.5 GHz in this case. As the fractal iteration increases, the reflection coefficient ($S_{11}$, dB) shows an increase in the second passband bandwidth, from 770 MHz for the 0th iteration to 1.47 GHz for the 5th iteration, which accounts for a 190% improvement in bandwidth by utilizing this fractal structure. The $S_{21}$ plot shows comparable minimum passband $S_{21}$ losses for all iterations of approximately $-1$ dB. The third passband show a larger variation in frequency range between 6 GHz to 8.5 GHz as iteration order increases from 0th to 5th order. This is due to the resonant lengths within the fractal stub becoming shorter and greater in number.

## 3. SYMMETRIC H-FRACTAL FILTER

Figure 3 shows the four different 5th order (Fig. 2(a)) H-fractal filter configurations which are explored throughout the paper. The cases where all T-junctions have symmetric branch lengths are referred as the symmetric filter. When the scaling factor $R_{scale}$ is not equal to unity, the branching is not symmetric and the fractal topology is referred as asymmetric. The fractal structure itself is parameterized by fractal iteration, fractal scale, $w_{scale}$, and $L_{scale}$. For all of the following designs, the filter uses a 60 mil FR-4 substrate with a relative dielectric permittivity of 4.4. The main 50 $\Omega$ microstrip transmission line is 2.9 mm wide using a 0.675 mil thick copper trace.

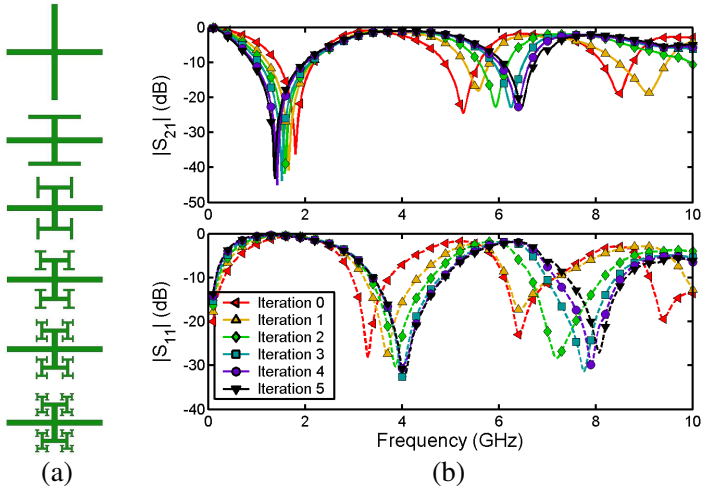


**Figure 2.** Fractal iteration from 0th to 5th (top to bottom) shown in (a), with associated magnitude of the scattering parameters shown in (b), $S_{21}$ (top) and $S_{11}$ (bottom) for the zero offset symmetrical filter, where total length from the main transmission line to open stub is kept constant.

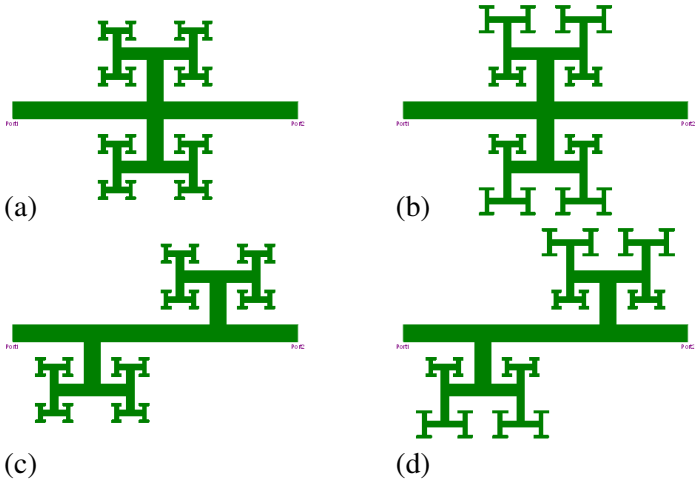


**Figure 3.** Four different configurations of the H-fractal filter, the (a) symmetric zero offset, (b) asymmetric zero offset, (c) symmetric with offset, and (d) asymmetric with offset cases.

### 3.1. Zero Offset

The symmetric zero offset configuration is illustrated in Fig. 3(a). Fractal scale was also investigated, but was shown to have little effect on the resonances throughout the frequency range as shown in Fig. 4(a). The choice of scale is determined by the desired level of compactness and the manufacturability.

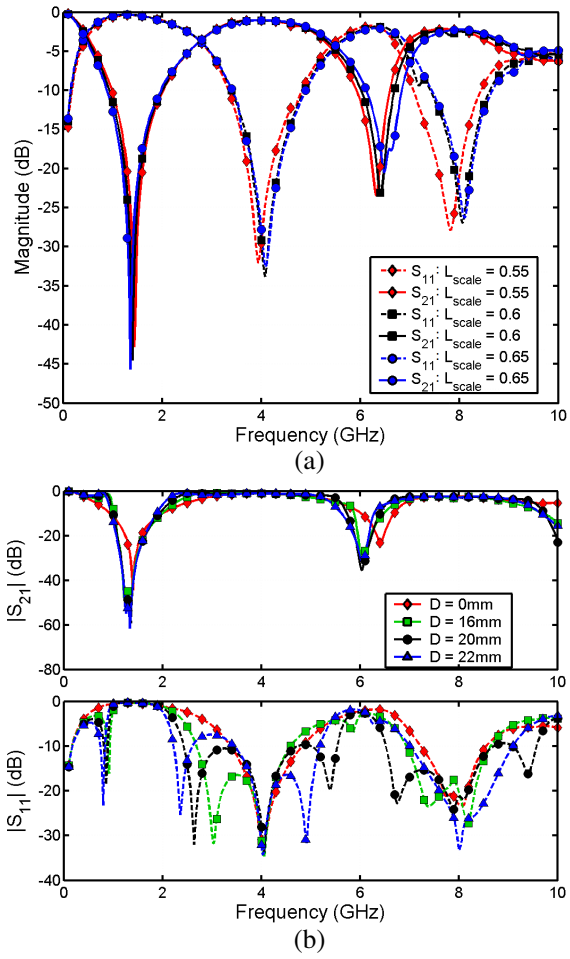


**Figure 4.** The magnitude of the scattering parameters, $S_{21}$ (top) and $S_{11}$ (bottom), for the parametrization of the zero offset symmetric filter (topology of Fig. 3(a)) for the parameters. (a) $L_{scale}$ from 0.55 to 0.65 and (b) $D$ from 0 mm to 22 mm (producing topology of Fig. 3(c)).

### 3.2. Stub Offset

In a multi-stub filter such as this, stub offset is a determining factor on the shape of the filter response. Consider the first stub and $50\,\Omega$ port as a single load. The second stub and interconnecting line act as a single stub matching transformer. Therefore, the offset between the stub and load determines the level of matching at different frequencies. It is evident from Fig. 4(b) that as the offset $D$ approaches a quarter wavelength of the design frequency, additional resonances enter the passband. These resonances approach from the upper end of the band and shift lower as the offset is increased. At an offset of $D = 20\,\text{mm}$, very near the quarter wavelength value, there is an optimal passband response containing three such resonances, allowing the second passband 3 dB bandwidth to be increased from 1.5 GHz in the zero offset case to 3.1 GHz in the optimal case. The passband insertion loss, $S_{21}$, remains under 2 dB, with a less than 1 dB minimum. The trade-off is an increase of 20 mm in filter length. Further, the second passband centered near 8 GHz shows a 3 dB impedance bandwidth from 6.8 GHz to 8.57 GHz but the passband loss, $S_{21}$, has slightly increased because the same physical length of the transmission lines are now electrically larger causing higher losses.

### 3.3. Fractal vs. Straight Stub

Notice that fractal iteration zero is simply a conventional straight stub filter. Such filters rely on the resonances of the stub to produce a desired filter response. Comparing the straight stub filter to a 5th order fractal stub filter, as shown in Fig. 5, a significant increase in the second and third passband bandwidths can be seen while the first passband has a smaller bandwidth and higher reflection coefficient. The straight stub filter's second passband consists of three individual resonances where the $S_{11}$ is greater than $-10\,\text{dB}$ between them. By contrast, the 5th order filter benefits from a single band from 2.3 GHz to 5.5 GHz where the reflection coefficient $S_{11}$ is below $-10\,\text{dB}$, accounting to 82% of the fractional bandwidth and resulting in lower insertion loss in this passband. Another benefit of this fractal structure is filter width reduction. For the responses plotted in Fig. 5, the filter width was reduced by 9.3 mm (normal to the main transmission line) per side, where the straight stub length was originally 23.8 mm per side. Filter length on the other hand increases, resulting in a filter with comparable area requirements but a modified aspect ratio with regards to the area use. This may be useful in some form factor requirements.

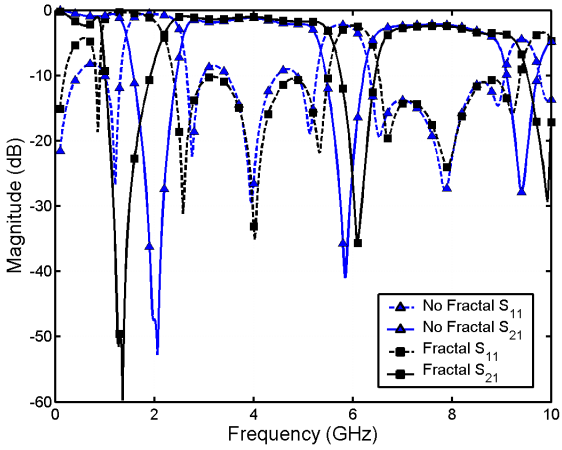


**Figure 5.** Comparison of the scattering parameters, $S_{21}$ and $S_{11}$, of the H-fractal filter (topology of Fig. 3(c)) compared to a non-fractal stub of equivalent length (0th order).

## 4. ASYMMETRIC H-FRACTAL FILTER

An advantage of the H-fractal design is the ability to introduce novel defects into the structure to produce a new filter response. Here, asymmetry was introduced in the basic fractal pattern of Fig. 3(a), as described in Section 3, creating the novel asymmetrical fractal geometry of Fig. 3(b). As shown in Fig. 6(a), the asymmetry causes another resonance which provides a notch band in the middle of the second passband of the symmetrical fractal filter. Fig. 6(b) shows the magnitude current distribution which clearly shows a resonance in the asymmetrical portion of the H-fractal filter. The resonance in the asymmetrical portion of the filter causes reflection of the energy from the input so as to not pass it from the input to the output.

The asymmetry in the H-fractal design was then parametrized and optimized. Just as was performed with the symmetrical filter (Fig. 3(a)), the fractal scale parameter was modified to characterize its effects on the asymmetric H-fractal filter. The results are shown in Fig. 7(a), where $L_{scale}$ was changed from 0.5 to 0.65 with $R_{scale}$ fixed at 1.5. Altering $L_{scale}$ clearly moves the asymmetry created notch, with a higher fractal scale moving the notch down in frequency and the lower fractal scale moving the notch band up in frequency. This is due to the shorter asymmetrical segment at lower fractal scale values. Three useful points are notable about Fig. 7(a): Changing the fractal

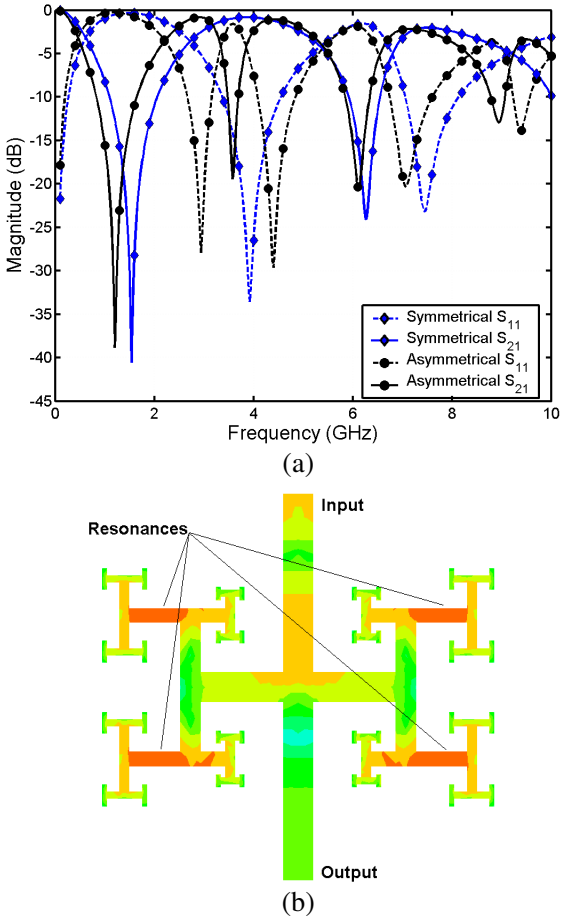


**Figure 6.** (a) Comparison of the scattering parameters, $S_{21}$ and $S_{11}$, between the zero offset symmetric and asymmetric fractal stubs (topologies of Figs. 3(a) and 3(b), respectively), and (b) the current magnitude plot showing the resonance in the asymmetric branch responsible for producing the notch at 3.6 GHz.

scale does not move the preexisting pass and notch bands significantly, the 3 dB notch bandwidth is not affected greatly, and the magnitude (depth) of the notch is not affected greatly. This demonstrates the tuning benefit where changing fractal scale can be used to isolatedly move the center frequency of the notch. Since the filter now affords for the asymmetrical scaling with $R_{scale}$, this parameter was also modified

to see its effects. The results are shown in Fig. 7(b), where the asymmetry scale was changed from 1.4 to 2 while the fractal scale was fixed at 0.5. Altering the asymmetrical scale clearly moves the notch in both center frequency and magnitude, and changes the −3 dB notch bandwidth. As asymmetry scale increases, the portion of microstrip which resonates becomes longer causing the shift of the notch lower in frequency. Again it is clear that the preexisting notch- and pass- bands are not greatly affected by changing asymmetry scale, demonstrating the isolated tuning benefit of the asymmetrical fractal filter.

As conducted with the symmetrical analysis (Fig. 3(c)), the two sides of the asymmetric H-fractal filter (Fig. 3(d)) were offset for improved filter characteristics. Fig. 7(c) shows the results of changing the offset from 18 mm to 24 mm. It can be seen that the center frequencies of the notch, pass, and stop bands remain constant, but the bandwidth and $S_{11}$ match change dramatically over swept length. Here the term stop bands are reserved for the wider rejected bands at around 1 GHz and 6 GHz which are present in both symmetrical and asymmetrical topologies, while the term notch band is reserved for the narrower rejected band created by the asymmetrical fractal structure. With a −10 dB acceptable $S_{11}$ match, the optimum bandwidth versus match is found to be with approximately $D = 22$ mm offset distance. Fig. 7(c) shows a significant improvement over Fig. 7(b) in terms of filter $Q$, optimizing the pass and stop bands.

This warranted further investigation of the fractal scale and asymmetry scale with the optimized offset filter topology, and offset $D = 22$ mm. Fig. 8(a) shows the effects of $L_{scale}$ on the optimized offset filter, with the values for $L_{scale}$ being swept from 0.50 to 0.65

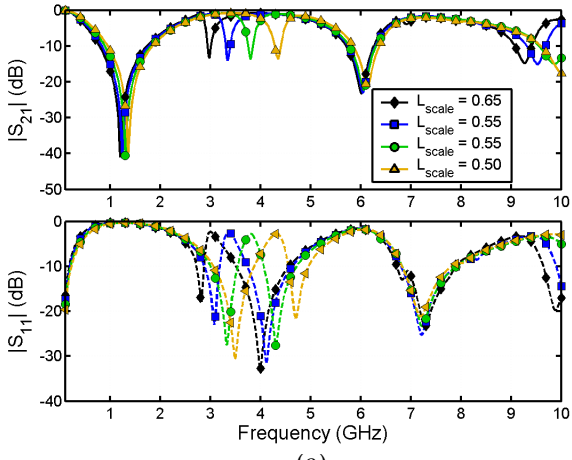


(a)

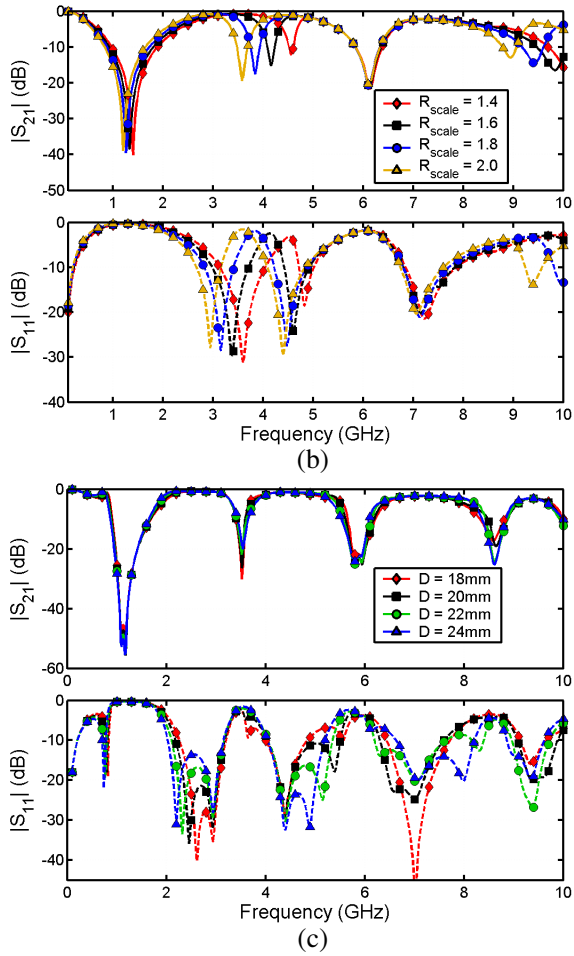


**Figure 7.** The magnitude of the scattering parameters, $S_{21}$ (top) and $S_{11}$ (bottom), for the parametrization of the zero offset asymmetric filter (topology of Fig. 3(b)) for the parameters: (a) $L_{scale}$ from 0.50 to 0.65 ($R_{scale} = 1.5$), (b) $R_{scale}$ from 1.4 to 2.0 ($L_{scale} = 0.50$), and (c) $D$ from 18 mm to 24 mm (producing topology of Fig. 3(c) with $R_{scale} = 2.0$ and $L_{scale} = 0.5$).

while $R_{scale}$ is fixed at 1.5. These results are similar to the non-offset asymmetrical (Fig. 3(b)) results, but slightly affects the notch 3 dB bandwidth and the location of the pre-existing notch bands. As the scale is decreased, the notch shifts higher in frequency, its

3 dB bandwidth increases, and the pre-existing notch bands also move resulting in an increase of the second passband bandwidth of around 200 MHz. Fig. 8(b) shows the effects of $R_{scale}$ on the optimized offset filter configuration, with $R_{scale}$ being changed from 1.4 to 2 while $L_{scale}$ is fixed at 0.55. These results are similar to the non-offset asymmetrical filter (Fig. 3(b)) results, where the notch magnitude (depth) and center frequency changes. In all passbands, the $S_{11}$ is better than $-10$ dB, with a slight increase in second passband bandwidth as $R_{scale}$ increases.

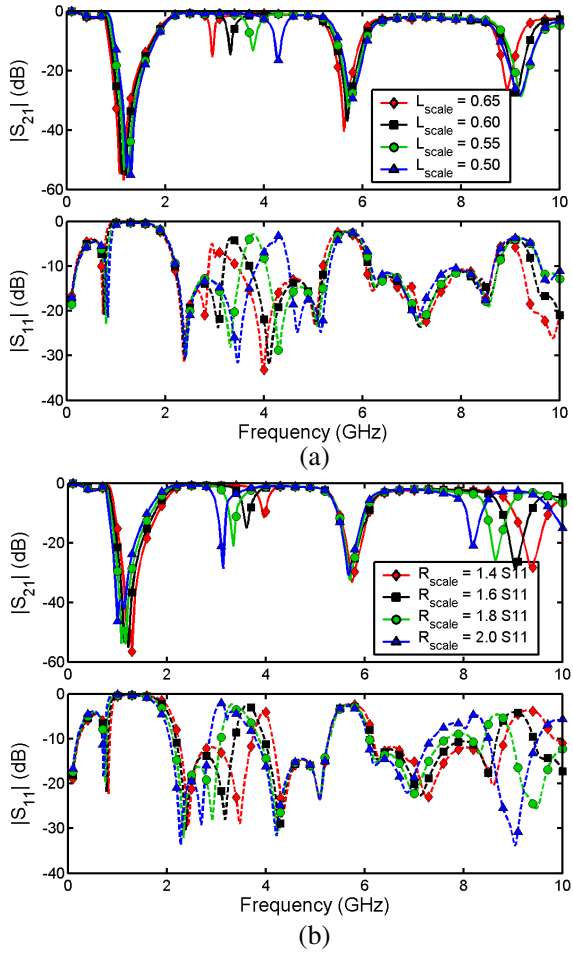


**Figure 8.** The magnitude of the scattering parameters, $S_{21}$ (top) and $S_{11}$ (bottom), for the parametrization of the offset asymmetric filter (topology of Fig. 3(d), $D = 22$ mm) for the parameters: (a) $L_{scale}$ from 0.5 to 0.65 ($R_{scale} = 1.5$), and (b) $R_{scale}$ from 1.4 to 2.0 ($L_{scale} = 0.55$).

## 5. EQUIVALENT CIRCUIT MODEL

An equivalent circuit model of the H-fractal filter can be developed and implemented in MATLAB for approximate analysis. In order to develop an equivalent circuit model of the filter, it is appropriate to begin with well known equations for effective permittivity, $\epsilon_{eff}(0)$, and microstrip impedance, $Z_m$, as taken from [14]. Since the filter performance is considered over a large range of frequencies, the frequency dependent form of the effective permittivity, $\epsilon_{eff}(f)$, developed by Kobayashi and as stated in [14] is used. Also important are the loss contributions, $\alpha_d$ and $\alpha_c$, from the dielectric substrate and conductive elements [15].

Each segment of the filter is a section of microstrip transmission line. Starting from an open end of the fractal stub, the load can be transformed to the center of the T-junction and added in parallel with the impedance on the other side of the T-junction. This is done repeatedly until the main line is reached, where the fractal stub impedance is added in parallel with the filter load and transformed down the line to the next stub. However, parasitic reactances associated with the T-junction itself must also be accounted for, since the junction disturbs the current distribution. Fig. 9 shows the basic circuit model of the T-junction consisting of series inductances and a shunt capacitance. This model assumes a width symmetric junction, which is true for the H-fractal filter under consideration. The shunt capacitance $C_T$ can be calculated using Equation (1) found in [16]. The series inductances are found using the semi-empirical Equations (2) and (3) given in [16].

$$C_{T,i} = \left(\frac{2w_{eff,i}}{\lambda_{g,i}} - 1\right)\frac{w_{eff,i}}{Z_{m,i+1}}\frac{\varepsilon_{eff,i}}{2\pi c} \tag{1}$$

$$L_{1,i} = -w_{eff,i+1}\left[\frac{w_{eff,i+1}}{h}\left(-0.016\frac{w_{eff,i}}{h} + 0.064\right) + 0.016\frac{h}{w_{eff,i}}\right]L_{w,i} \tag{2}$$

$$L_{2,i} = h\left[\frac{w_{eff,i+1}}{h}\left(0.12\frac{w_{eff,i}}{h} - 0.47\right) + 0.195\frac{w_{eff,i}}{h} - 0.357 + 0.283\sin\left(\pi\frac{w_{eff,i}}{h} - 0.75\pi\right)\right]L_{w,i} \tag{3}$$

The parameter $L_{w,i}$ is the inductance per unit length of the microstrip line. Also, the index $i$ refers to the T-junction where $i = 1$ is the first stud segment protruding from the main line as depicted in Fig. 9.

Finally, some change in phase reference planes is needed as a result of the modified current distribution at the center of the junction. The phase plane positions are illustrated in Fig. 10. Any offset in these phase planes should be subtracted from the lengths of each

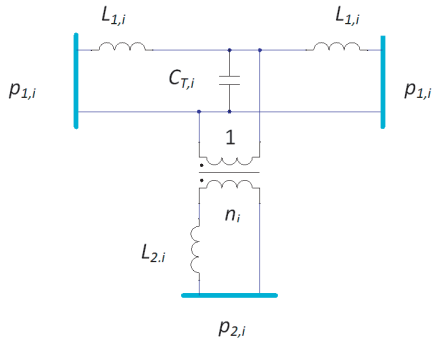


**Figure 9.** Circuit diagram showing the parasitic reactances $L_1$, $L_2$, and $C_T$ of the microstrip T-junction.

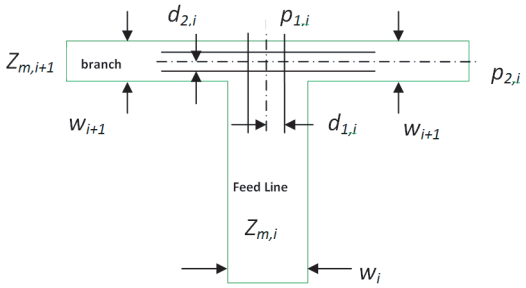


**Figure 10.** Schematic of microstrip T-junction showing the modified phase plane positions $d_1$ and $d_2$.

segment of the fractal. When the loads are transformed down each of these lengths, they must see the proper change in phase as defined by the modified reference plane positions $d_{1,i}$ and $d_{2,i}$ [16]. Thus, Equations (4) and (5) are used in the determination of transmission line length to compensate for the modified reference planes where Equation (6) defines $n_i^2$. Reference [16] also mentions that the equation for $d_{2,i}$ often overestimates the shift in reference plane especially at microwave frequencies.

$$d_{1,i} = 0.05 w_{eff,i+1} \frac{Z_{m,i}}{Z_{m,i+1}} n_i^2 \tag{4}$$

$$d_{2,i} = 0.5w_{eff,i} - w_{eff,i}\left\{\left[0.076 + 0.2\left(\frac{2w_{eff,i}}{\lambda_{g,i}}\right)^2 + 0.663\exp\left(-1.71\frac{Z_{m,i}}{Z_{m,i+1}}\right)\right] - 0.172\ln\left(\frac{Z_{m,i}}{Z_{m,i+1}}\right)\right\}\frac{Z_{m,i}}{Z_{m,i+1}} \quad (5)$$

$$n_i^2 = \left[\frac{\sin\left(\pi\dfrac{w_{eff,i}}{\lambda_{g,i}}\dfrac{Z_{m,i}}{Z_{m,i+1}}\right)}{\pi\dfrac{w_{eff,i}}{\lambda_{g,i}}\dfrac{Z_{m,i}}{Z_{m,i+1}}}\right]^2\left[1 - \left(\pi\frac{d_{2,i}}{\lambda_{g,i}}\right)^2\right] \quad (6)$$

In the following section, we will compare the $S$-parameter data for the circuit model, numerical simulation, and fabricated versions of the final design.

## 6. FABRICATION AND EXPERIMENTAL VERIFICATION

The asymmetrical H-fractal filter design was optimized for a potential WiMAX/WiFi transponder application where the center frequency of the notch would correlate with the WiMAX 3.5 GHz band operation. In such an application, WiFi could be relayed by the transponder over WiMAX to another local area network (LAN) which is further than WiFi would be able to reach. If placed in the WiFi signal path, this filter could help to block out the WiMAX transmit frequency at 3.5 GHz band while still receiving and transmitting at 2.4 GHz and 5 GHz WiFi bands, helping to solve the co-site interference problem and allowing the use of one ultra wide band antenna for both WiFi bands.

To facilitate this application, a more realistic model of an asymmetric H-fractal filter was built using Ansoft's HFSS. The substrate used was a low cost FR-4 (dielectric constant of 4.4 and loss tangent of 0.02) substrate of 60 mil thickness and $50 \times 30\,\text{mm}^2$ in area. Copper was used as the filter conductor with 0.675 mil thickness, which is well above the skin depth requirement and close to the thickness of the available copper clad FR-4. Two $50\,\Omega$ end launching SMA ports were included as part of the filter simulation model with dimensions matching those commercially available. Using the sweep data for $L_{scale}$ and $R_{scale}$, the filter scale factors were tuned to achieve a $-20$ dB notch band at 3.5 GHz while the stub offset was also adjusted to maintain an optimal passband response. The final values for $L_{scale}$ and $R_{scale}$ were 0.5 and 2, respectively, while the distance between fractal stubs, $D$, was 22.5 mm. The photograph of the fabricated asymmetric H-fractal filter prototype is shown in Fig. 9(a).

For measurement of the filter, Anritsu's Vector Network Analyzer model number 37269D was used after proper calibration procedures, which is available in the Antenna and Microwave Laboratory (AML) at San Diego State University. Fig. 9(b) shows the $S$-parameter plots for both the fabricated and simulated versions of the filter with the pass, and notch band sections delineated for clarity. The fabricated filter's first two passbands ($S_{11} = -10\,\text{dB}$) are from 2.09 GHz to 3.18 GHz (fractional bandwidth of 1.09 GHz, 41.36%) and from 4.1 GHz to 5.43 GHz (factional bandwidth of 1.33 GHz, 27.91%), both for WiFi application along with a notch band ($S_{21} = -3\,\text{dB}$) from 3.3 GHz to 3.94 GHz (factional bandwidth of 0.64 GHz, 17.67%). The higher frequency end pass bands are grayed out as they offer slightly higher insertion loss which may not be acceptable, which is attributed to the lossy nature of FR-4 substrate. Considering all these passbands, the filter offers multi-passband response with a tuned notch band. However, very good agreement is observed between the fabricated and simulated filter below 5 GHz where properties of the FR-4 substrate are well known. The circuit model predicts the return loss and location of the notch band in agreement with both simulation and measurement. As previously mentioned in Section 5, the phase plane adjustment $d_2$ overestimates at microwave frequencies and was therefore scaled by a factor of 0.3. The circuit model transmission coefficient predicts larger bandwidth for passbands 1 and 2. There is also considerable disagreement in both the reflection and transmission coefficients of the circuit model as in the lossy region. We can attribute these disagreements to higher order effects not included in the circuit model such as the coupling capacitances between nearby branches and feedlines of each T-junction. Additionally, the circuit model shows ripples in the $S_{21}$ passband above 0 dB, which is an unphysical effect we attribute to assumptions in the T-junction model itself. As the permittivity of the FR-4 decreases with the increase in frequency, the measured resonances in the $S$-parameters are shifted slightly. The measured $S_{11}$ shows some disagreement from the simulated data towards the end of the frequency band. This is attributed to the inaccurate modeling of the low cost FR-4 substrate material where its properties are not well behaved. The depth and location of the notch in the second passband is very close to the simulated value.

Although the novelties of this design are more prominently the tuned notch band created by the asymmetry and the analytics behind the design, the bandwidths of this filter compares with other wideband filters in the literature. The passband bandwidths of 41.36% and 27.91% compare well against the fractal filter found in [5] with a 48% bandwidth, and even the non-fractal filter designed in [7] having 39%,

20%, and 27% bandwidths. Furthermore, this design shows a great improvement over the work in [11], where the percent bandwidths are not listed, but the −10 dB bandwidths for the passbands appear to be 30% maximum.

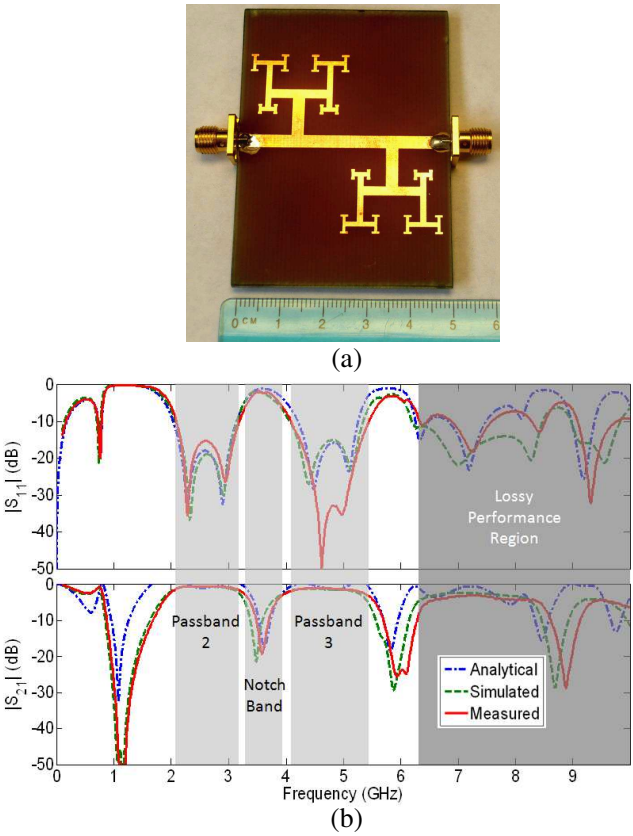


**Figure 11.** (a) Photograph of the fabricated prototype of the microstrip H-fractal filter and (b) the magnitude of the scattering parameters, $S_{21}$ and $S_{11}$, comparing the measured, simulated and analytical results for the fabricated filter showing the notch band at 3.5 GHz for a potential WiMAX/WiFi application.

## 7. CONCLUSION

This paper presented the investigation results of a microstrip H-fractal based wideband multi-passband filter with a tuned notch band. An

extensive parametric study was performed on four different fractal based filter configurations and their effect on the filter response was noted. The symmetric filter with stub offset showed improved bandwidth and $S_{11}$ performance over a double straight stub filter of the equivalent length. A novel asymmetry was introduced in scaling of branches at the T-junction, which produced a tunable notch band in the second passband. Finally, a filter was designed, fabricated, and measured on a low cost FR-4 substrate material for a potential WiMAX/WiFi transponder application requiring a notch band at 3.5 GHz. The fabricated filter's measured $S$-parameters were in good agreement with simulated ones except towards the end of the frequency band, where the substrate properties of the low cost FR-4 material are not well behaved.

## ACKNOWLEDGMENT

The authors would like to acknowledge Justin Church and Ashish Tuteja at San Diego State University for their contributions to this research.

## REFERENCES

1. Kim, I. K., N. Kingsley, M. Morton, R. Bairavasubramanian, J. Papapolymerou, M. M. Tentzeris, and J.-G. Yook, "Fractal-shaped microstrip coupled-line bandpass filters for supression of second harmonic," *IEEE Transactions on Microwave Theory and Techniques*, Vol. 53, No. 9, 2943–2948, September 2005.
2. An, J., G.-M. Wang, W.-D. Zeng, and L.-X. Ma, "UWB filter using defected ground structure of von koch fractal shape slot," *Progress In Electromagnetics Research Letters*, Vol. 6, 61–66, 2009.
3. Weng, M.-H., L.-S. Jang, and W.-Y. Chen, "A sierpinski-based resonator applied for low loss and miniaturized bandpass filters," *Microwave and Optical Technology Letters*, Vol. 51, No. 2, 411–413, February 2009.
4. Church, J., D. West, P. Dagar, and S. K. Sharma, "A novel wideband microstrip fractal bandpass filter with a notch band at 5–6 GHz," *Microwave and Optical Technology Letters*, Vol. 52, No. 6, 1413–1416, June 2010,
5. Xiao, J.-K. and Q.-X. Chu, "Novel microstrip trangular resonator bandpass filter with transmission zeros and wide bands using fractal-shaped defection," *Progress In Electromagnetics Research*, Vol. 77, 343–356, 2007.

6. Tong, F. and H. W. Liu, "Fractal-shaped microstrip dual-mode bandpass filter with asymmetrical sinuous spurlines," *Microwave and Optical Technology Letters*, Vol. 51, 745–747, 2009.
7. Baral, R. N. and P. K. Singhal, "Design of microstrip band pass fractal filter for suppression of spurious band," *Radioengineering*, Vol. 17, No. 4, 34–38, December 2008.
8. Crnojevic-Bengin, V. and D. Budimir, "Novel compact microstrip resonators with multiple 2-D hilbert fractal curves," *European Microwave Conference*, Vol. 1, October 2005.
9. Chen, W.-L., G.-M. Wang, Y.-N. Qi, and J.-G. Liang, "Fractal-shaped stepped-impedance transformers for wideband application," *Microwave and Optical Technology Letters*, Vol. 49, 1628–1630, 2007.
10. Chen, W.-L., G.-M. Wang, and Y.-N. Qi, "Fractal-shaped Hi-Lo microstrip low-pass filters with high passband performance," *Microwave and Optical Technology Letters*, Vol. 49, No. 10, 2577–2579, 2007.
11. Chen, D., S. Wang, L. Li, Z. Y. Liu, and X.-Z. Zhao, "Microstrip filter with H-shaped fractal," *Applied Physics Letters*, Vol. 88, 1–3, 2006.
12. Wen, W. J., L. Zhou, J. S. Li, W. K. Ge, C. T. Chan, and P. Sheng, "Subwavelength photonic band gaps from planar fractals," *Physical Review Letters*, Vol. 89, 1–4, 2002.
13. Ansoft Corporation, *Designer V4.0 and High Frequency Structure Simulator (HFSS) V11.0*.
14. Gupta, K. C., R. Garg, and I. Bahl, *Microstrip Lines and Slotlines*, 2nd edition, Chapter 1, Artech House, Boston, London, 1996.
15. Gupta, K. C., R. Garg, and I. Bahl, *Microstrip Lines and Slotlines*, 2nd edition, Chapter 2, Artech House, Boston, London, 1996.
16. McEwan, N. J., T. C. Edwards, D. Dernikas, and I. Glover, "Signal transmission, network methods, and impedance matching," *Microwave Devices, Circuits, and Subsystems for Communications*, I. A. Glover, S. R. Pennock, and P. R. Shepherd (eds.), John Wiley and Sons, 2005.
17. Moghadasi, S. M., A. R. Attari, and M. M. Mirsalehi, "Compact and wideband 1-D mushroom-like EBG filters," *Progress In Electromagnetics Research*, Vol. 83, 323–333, 2008.